# Novel Nanostructured $SiO_2/ZrO_2$ Based Electrodes with Enhanced Electrochemical Performance for Lithium-ion Batteries

DongWoong CHOI [(1) (2)], Kwang-Leong CHOY [(1)]*

(1) UCL Institute for Materials Discovery, (2) Department of Chemistry
University College London, WC1E, 7JE, United Kingdom
*Corresponding author: k.choy@ucl.ac.uk

**Abstract**

In this article, a novel anode material with high electrochemical performance, made of elements abundant on the Earth, is reported for use in lithium ion batteries. A chemically synthesised material ($SiO_2/ZrO_2$) containing Si-O-Zr bonds, exhibits as much as 2.1 times better electrochemical performance at the $10^{th}$ cycle than a physically mixed material ($SiO_2$+$ZrO_2$) of the same elements. When compared to synthesized $SiO_2$ or conventional graphite-based electrodes, the $SiO_2/ZrO_2$ anode shows superiorcapability and cycling performance. This superior performance is ascribed to the effect of ternary compounds, which contributes not only to increasing the packing density, but also to creating the Si-O-Zr bond that makes additional reactions between $SiO_2/ZrO_2$ and lithium ions possible. The Si-O-Zr bond also contributes to improved conductivity for SSZ and provides facile paths for charge transfer at the electrode/electrolyte interface. Therefore, the overall internal resistance in a battery would be decreased and better performance could thus be obtained, with this type of anode. In every result, the positive influence of the Si-O-Zr bonds in the anode of a lithium ion battery was confirmed.

**Keywords**

$SiO_2$; $ZrO_2$; Ternary compound; Si-O-Zr bond; Lithium ion batteries

## Introduction

Lithium ion battery (LIB) technology has attracted great attention as an alternative energy source since the introduction of the first commercial LIB in 1991 [1-3]. LIBs have

high energy/power density, long lifespan, and a wide range of modern applications, from portable devices to electric vehicles (EV). Generally, graphitic carbon has been used as the commercial anode material for LIBs; however, when compared to other promising materials, it is very limited by its low theoretical specific capacity. In addition, commercial electronics have also quickly developed many convenient embedded functions that increase device power consumption. As a result, there is a strong commercial demand for improved LIB energy storage performance to meet increasing energy requirements [4]. To address this issue, diverse LIB research is currently underway, including development of new anode materials.

Currently, the best known host material $SiO_2$, and SiO or $ZrO_2$ is the material added to support the host material. Zhang et al. fabricated and tested materials of different $SiO_2$ content (0, 5, 10, 15, and 20 wt %), and the film with 15 wt% $SiO_2$ showed the best cycling stability. NiS@$SiO_2$/graphene with a hierarchical architecture was fabricated by Zhang et al., and this electrode showed good electrochemical capacity and cyclability performance at 50 $^oC$ [5]. Nan et al. reported fabricating porous carbon nanofibers (PCNFs) by carbonization of electrospun PI/$SiO_2$ hybrid nanofibers. The PCNFs exhibited a capacity of 730mAh $g^{-1}$ and a large specific surface area (950 $m^2$ $g^{-1}$) [6]. Yao et al. established that $SiO_2$ coated on carbon would support high storage capacity as well as alleviate volume change during lithium insertion and extraction, and they attributed this to the effects of $Li_2O$ or $Li_4SiO_4$ [7]. It is known that inert $Li_2O$ is formed by a reaction of lithium ions with metal oxide. This $Li_2O$ can help to maintain the active material and reduce volume change, thus enhancing cyclability. A $SiO_2$/Cu/PAN-C composite was prepared by Li et al. and this composite exhibited the specific capacity of 537 mAh $g^{-1}$ with the buffer effect of Cu and PAN/C [8]. In a material with the structure of a core within a shell (Si/SiO), the shell SiO formed lithium silicates that acted as a buffer to reduce the volume change in the core Si, and therefore, the cyclabilty was clearly enhanced [9]. Liu et al. reported that a $ZrO_2$ coating in $Li_4Ti_5O_{12}$ effectively improved the performance of the active anode material by suppressing SEI formation and enhancing electron transport [10]. Spinel $Li_4Ti_{5-x}Zr_xO_{12}$ ($0 \leqslant x \leqslant 0.25$) was synthesized using a solid state reaction method, from $Li_2CO_3$, $ZrO_2$, and $TiO_2$ as raw materials. The authors of the study claimed that Zr-doped materials had better reversibility than that of pristine $Li_4Ti_5O_{12}$ (i.e., the Zr doping was beneficial to the reversible intercalation and de-intercalation of the lithium ion). Pristine $Li_4Ti_5O_{12}$ and $Li_4Ti_{4.9}Zr_{0.1}O_{12}$ delivered about 111 mAh $g^{-1}$ and 172 mAh $g^{-1}$, respectively, at a charge/discharge rate of 2 C [11].

The insertion and extraction mechanisms of lithium ions in $SiO_2$ have been investigated, and Sun et al. suggested the two reversible reactions below in (1) and (2). The other mechanisms claimed by Guo et al. are shown in (3), (4), and (5). It is known that reactions (3) and (4) are irreversible, and that (5) is a reversible reaction. Depending on the $SiO_2$ particle size, the reaction pattern can switch between the mechanisms of (3)➔(5) with large particles and (4)➔(5) with small particles.

$$5SiO_2 + 4Li^+ + 4e^- \rightarrow 2Li_2Si_2O_5 + Si \quad (1)$$

$$Si + xLi^+ + xe^- \leftrightarrow LixSi \quad (2)$$

$$SiO_2 + 4Li^+ + 4e^- \rightarrow 2Li_2O + Si \quad (3)$$

$$2SiO_2 + 4Li^+ + 4e^- \rightarrow Li_4SiO_4 + Si \quad (4)$$

$$Si + xLi^+ + xe^- \leftrightarrow LixSi \quad (5)$$

$SiO_2$ is a major constituent of sand and one of the most abundant substances in the Earth's crust. Thus, the cost of $SiO_2$ is much lower than that of most metal oxides. It also reacts with a low discharge potential and can store a large quantity of lithium ions. Meanwhile, $ZrO_2$ has the features of suppressing SEI formation and improving electron transport at the negative electrode. Therefore, the capacity of active materials can be enhanced with the support of $ZrO_2$.

Although many approaches utilizing metal oxide materials (e.g., $SiO_2$, $ZrO_2$, and $TiO_2$) have been carried out, as far as we know, there has been no published study regarding the effect of the Si-O-Zr bond between $SiO_2$ and $ZrO_2$, and the use of $SiO_2/ZrO_2$as anode material. Therefore, in this paper, this effect was investigated by synthesizing several materials ($SiO_2/ZrO_2$, $SiO_2$, and $ZrO_2$) by the sol-gel method. In addition, physically mixed particles of $ZrO_2$ and $SiO_2$ were also prepared from the synthesized $SiO_2$ and $ZrO_2$. Herein, SSZ, SS, and SZ represent ~~the~~ synthesized $SiO_2/ZrO_2$, $SiO_2$, and $ZrO_2$, respectively, while PSZ stands for the physically mixed material of SS and SZ ($SiO_2+ZrO_2$). A combination of FT-IR, XRD, TEM, EDS, and SEM were employed to determine the characteristics of these materials. The presence of the Si-O-Zr bond was confirmed using FT-IR. Films of these particles were uniformly dispersed by doctor-blade casting and then assembled into a cell. Finally, the electrochemical properties of the cell were measured, and then compared to a cell

using materials without a Si-O-Zr bond. Our hypothesis was that the separate advantages of $SiO_2$ and $ZrO_2$ mentioned above, would be combined in SSZ with Si-O-Zr bonding, and that this would provide enhanced capacity of the active materials via a synergistic effect. This has been confirmed experimentally, as described in this article.

## Experimental

### Preparation of materials

The SSZ was synthesized according to the available literature [12]: $ZrOCl_2 \cdot 8H_2O$ was dissolved in distilled water; then $(NH_4)_2CO_3$ was added until the precipitate of zirconyl carbonate formed. That precipitate was stirred in $(NH_4)_2CO_3$ solution until the pH reached 8. Then, the anionic surfactant sodium dodecylsulphate was added to the solution. After the mixture was stirred for 30min, sodium metasilicate solution (0.5 g/cc) was dripped into the mixture to form a semi-transparent gel. This gel was kept overnight and aged at 80 °C for two days and at 100 °C for one day. The final product was cooled and washed with distilled water several times to remove the surfactant; then the product was filtered. This mixed oxide was dried at room temperature and heated at 90 °C for 6 h; then calcined at 1050 °C for 6 h. $ZrO_2$ and $SiO_2$ were synthesized according to the methods described in the literatures, respectively [13, 14]. An ammonium hydroxide solution was dripped in a 0.2M $ZrOCl_2 \cdot 8H_2O$ solution until the pH reached 10. This solution obtained ($ZrO_2 \cdot nH_2O$ sol.) was washed with distilled water and dried at 110 °C for 10 h; then treated at 1050 °C for 3h. The $SiO_2$ was obtained from tetraethylorthosilicate (TEOS) in an ethanol medium, in the presence of ammonium hydroxide. The ethanol was taken and kept in a sonication bath. After 10 min, the required amount of TEOS was added for 20 min, and a 28% ammonium hydroxide solution was introduced as a catalyst to promote the condensation reaction. A physically mixed oxide of $SiO_2$ and $ZrO_2$ (PSZ: $SiO_2$+$ZrO_2$) was prepared by mixture of the synthesized $SiO_2$ (SS) and the synthesized $ZrO_2$ (SZ).

### Material characterizations

The synthesized materials were examined using Fourier Transform Infrared Spectroscopy (FT-IR, Spectra Two, Perkin Elmer). The FT-IR spectra were recorded over a wave number range of 4000 to 400 $cm^{-1}$. The crystalline structures of the materials were analyzed using an x-ray diffraction (XRD, STOE, STADI-P) device, equipped with a Mo-

Kα1 radiation emitter. Transmission electron microscopy (TEM, Jeol2100) with an acceleration voltage of 200kV and scanning electron microscopy (SEM, Jeol) were employed to perform the high resolution imaging. Energy dispersive X-ray spectroscopy and element mapping (EDS and EM, Oxford Instrument) were used to investigate the microstructure and the element distribution of the samples.

**Electrochemical characterization**

The electrochemical performance of the SSZ and PSZ powders was examined using a CR 2032 type cell. The negative electrode was prepared by doctor blade casting on Cu-foil. This viscous slurry contained a mixture of 50wt% synthesized materials, 20wt% graphite, 10wt% carbon black (super P, TIMCAL) and 20wt% poly-vinylidene fluoride (PVDF) in n-methylpyrrolidone (NMP). Li-metal foil was selected as the counter and reference electrodes. A solution of 1M $LiPF_6$ in ethyl carbonate and dimethyl carbonate (EC/DMC=1:1 volume ratio) was used as the electrolyte, and Whatman was applied as separator. Cells were assembled in a glove box filled with argon gas (maintained at <1ppm $H_2O$). Galvanostatic charge/discharge measurements were performed using an Arbin system within the potential range 0.001-2.0 V (vs. $Li/Li^+$) at various current densities. The loading density on copper foils was 2-3 $mg/cm^2$. Cyclic voltammetry was performed using the Arbin system between 0.001-2.0V at a scan rate of 0.05 mV/s. Electrochemical impedance spectra (EIS) were collected using Autolab, and impedance tests were carried out by applying AC voltage of 10mV over a frequency range from $10^{-1}$ to $10^5$ Hz.

## Result and Discussion

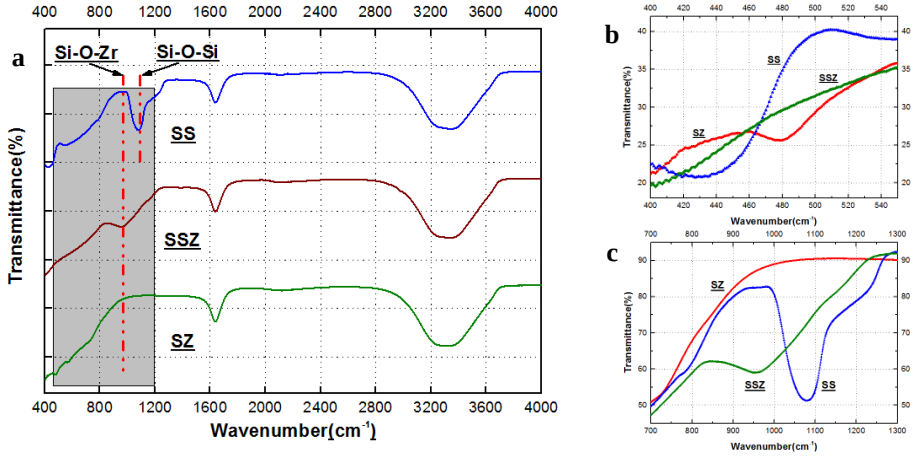


Figure 1. FT-IR of synthesized$SiO_2$ (SS), synthesized $ZrO_2$ (SZ), and synthesized $SiO_2/ZrO_2$ (SSZ) with Si/Zr molar ratio of '1' (a); Enlarged graph with the wave number range of 560 to 400 $cm^{-1}$ (b), and 1300 to 700 $cm^{-1}$ (c)

The FT-IR spectra of the SS, SSZ, and SZ particles are shown in Figure 1. The spectra of these samples were taken in the spectral range 4000 to 400 $cm^{-1}$. Overall, these FT-IR graphs were matched except for two ranges, shown in Figures 2-b and 2-c. In Figure 2-b, each SZ and SS band showed the observed frequency of vibration at 480 and 430 $cm^{-1}$. The SSZ curve appeared between the SZ and the SS curves. Although the band of SS at 1200 and 1080 $cm^{-1}$ and the band of SSZ at 955 $cm^{-1}$ were observed, the SZ band is not shown in Figure 2-c.Theband at 480 $cm^{-1}$ could be attributed to the stretching frequency of Zr-O in pristine zirconia. Two bands of SS at 780 and 430 $cm^{-1}$ were attributed to the Si-O-Si

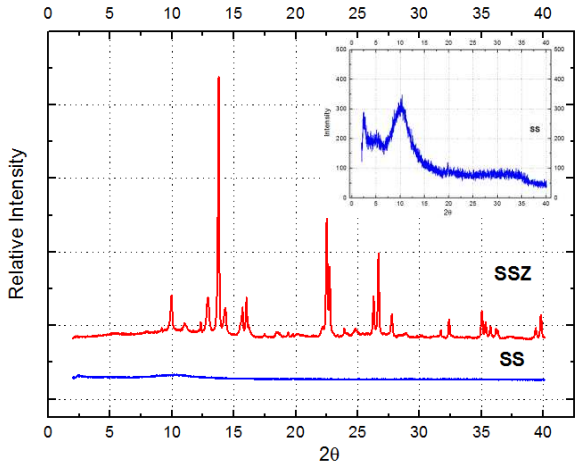


Figure 2. XRD patterns of synthesized $SiO_2/ZrO_2$ (SSZ) with molar ratio of Si/Zr=1, and synthesized $SiO_2$ (SS) at 1050 °C (inset: enlargement of synthesized $SiO_2$)

symmetric bond-stretching vibration and bond-bending vibration for pristine silica. The bands at 1200 and 1080 $cm^{-1}$ were associated with the Si-O-Si asymmetric bond stretching vibration [15]. The SSZ curve showed a peak of Si-O-Zr at 955 $cm^{-1}$, and this result matched those in other works [16-23]. The peak was caused by the formation of a silica network by the extraction of the zirconium atoms. The observation of the band at 1635 $cm^{-1}$ is attributed to absorbed water [15]. The broad band at 3400$cm^{-1}$ corresponded to the stretching of the OH group due to water in the samples [24]. Therefore, it could be concluded from the above that the particles of SSZ were prepared successfully with a Si-O-Zr bond.

The X-ray diffraction patterns of the SSZ, SS samples after calcination at 1050 °C for 6 h, and the results are showed in Figure 2. The SS showed amorphous, and the SSZ definitely exhibited crystalline structure. Broad peaks of SS are shown at the range of ′2θ’ = around 2.5 °and 10 °. The sharp peaks of SSZ, which are based on the broad bands of SS, are related to $SiO_2$. The rest of the peaks would be associated with $SiO_2/ZrO_2$ and $ZrO_2$.

The Energy Dispersive X-ray Spectroscopy (EDS) results were analyzed and mapped to evaluate the uniformity of distribution (Figure 3). The EDS analysis verifies each major component (Si, Zr, and O). (Please note that the copper (Cu) was from a metal holder, the carbon (C) was from a sample container sheet on the holder. Thus, these elements should be excluded.) Furthermore, the EDS mapping in Figure 3 shows that the Si, Zr, and O elements were all uniformly dispersed without agglomeration.

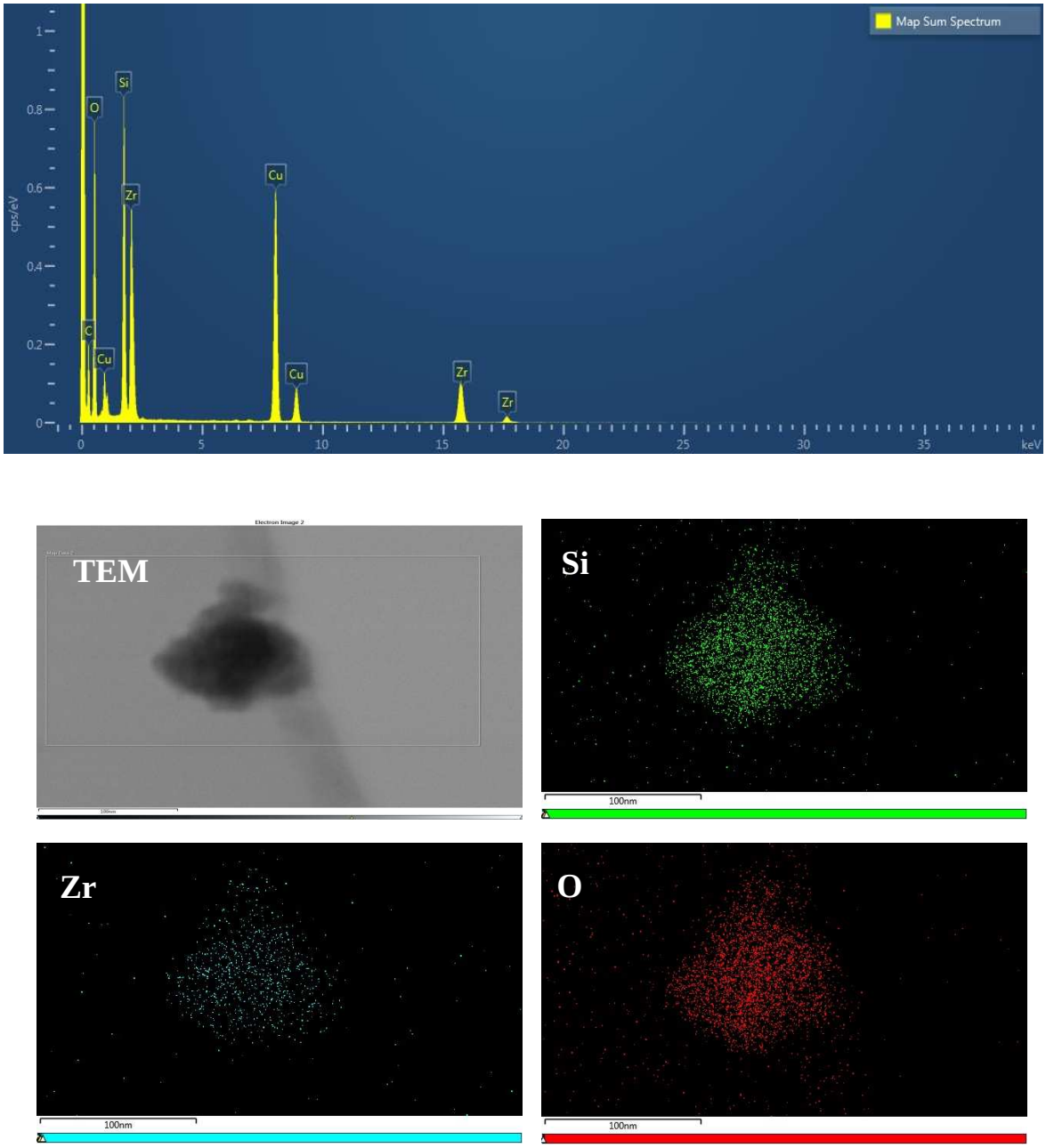


**Figure 3.** EDS analysis of the synthesized $SiO_2/ZrO_2$ (SSZ) nanoparticles: (Upper) Map sum spectrum (Note: copper (Cu) was from a sample holder, and carbon (C) was from a holder tape.); (Center left) TEM image of SSZ; Mapping analysis of TEM image for major elements (Si: center right, Zr: lower left, O: lower right)

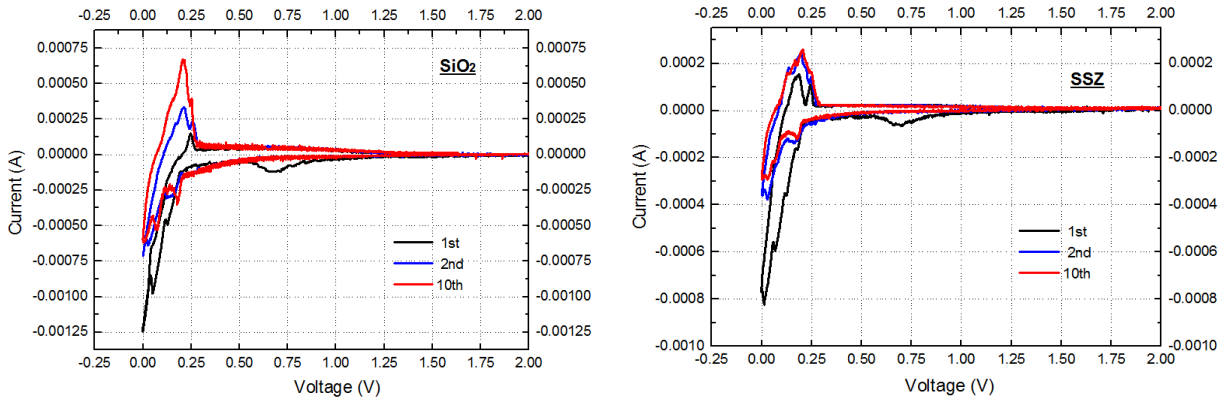


Figure 4. Cyclic voltammograms of synthesized $SiO_2$ (SS), synthesized $SiO_2/ZrO_2$ (SSZ) at a scan rate of 0.05 mV/s

Cyclic voltammograms (CVs) were investigated for the 1st, 2nd, and 10th cycles in order to understand the electrochemical behavior of the SS, and SSZ electrodes. The response of the corresponding CV, showing the reduction as negative and the oxidation currents as positive, is presented in Figure 4. Four cathodic peaks were observed at 1.4, 0.6, 0.126, and 0.049 V in the 1st cycle of SS, and five peaks (1.4, 0.6, 0.17, 0.124, and 0.069 V) were detected for SSZ. The first peak at 1.4 V, which was much broader and less discernable than the second peak at 0.6 V, was attributed to the beginning of the formation of the SEI layer [25]. The second peak is related to the formation of the SEI layer between the electrode and the electrolyte, and decomposition of the electrolyte. After the 1st cycle, the corresponding electrochemical reactions of these two peaks did not occur. This indicates that the SEI layer was mostly formed during the 1st cycle, and that those electrochemical reactions related to SEI formation were mainly irreversible. The shift of the third and the fourth peaks in SS might have been caused by the formation of a zirconium silicate network by the insertion of zirconium atoms in silica (0.126➔0.124 V and 0.049➔0.069 V). The peaks at 0.17 V in SSZ might be associated with a unique reaction of the SSZ electrode with ternary bonds. The anodic peaks were observed at 0.24 V in the SS, and at 0.18 and 0.24 V in the SSZ during the initial cycle. Those peaks correspond to the extraction of lithium ions from each electrode, in the de-alloying process. In the subsequent cycle, the previous single peak in SS was separated into two peaks. In the case of SSZ, the peaks located at 0.18 and 0.24 V become gradually combined and sharpened during the subsequent cycle process. According to the literature regarding $SiO_2$, the peak around 0.25 V is one of the oxidation peaks of Si during the extraction of lithium ions from $Li_xSi$ alloys [26, 27]. Therefore, the combined peak from 0.18

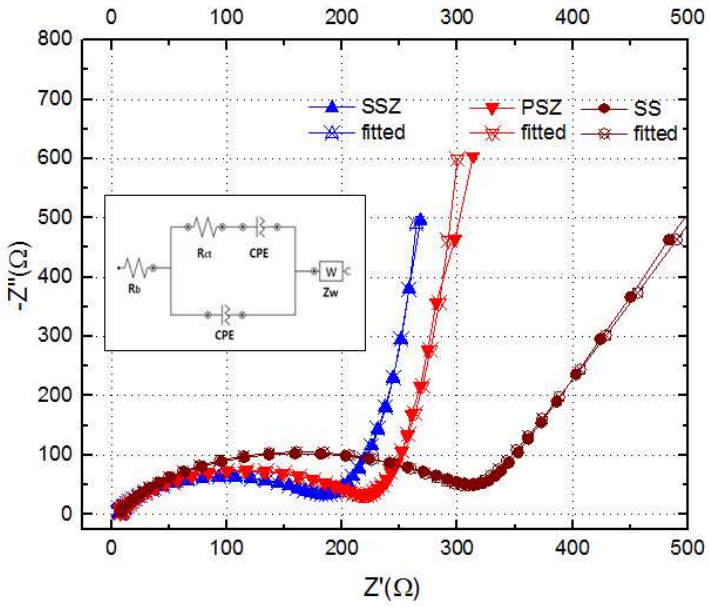


Figure 5. Electrochemical impedance of synthesized $SiO_2$(SS), $SiO_2/ZrO_2$(SSZ) and physically mixed $SiO_2$ + $ZrO_2$ (PSZ) (Inset: Equivalent circuit model for three electrodes)

Table 1. Summary of resistance value in each equivalent circuit

| Sample | Rb (Ω) | Rct (Ω) |
|---|---|---|
| SS | 5.93 | 309.39 |
| PSZ | 6.19 | 219.6 |
| SSZ | 5.63 | 181.86 |

and 0.24 V of SSZ could be associated with the oxidation reactions of the phase types of ZrSi during the extraction of lithium ions from Li-$SiO_2/ZrO_2$.

Electrochemical impedance spectra (EIS) were applied to understand the kinetic process of lithium-ion diffusion and electron transfer of the SSZ electrode with Si-O-Zr bonds. Figure 5 shows the Nyquist plots of each pristine electrode of SSZ and PSZ obtained in the frequency range between $10^{-1}$ to $10^{5}$ Hz, at the open circuit voltage. Both electrodes show similar impedance shapes, with one depressed semicircle at high frequency and an inclined line at low frequency. An equivalent circuit method was employed to fit the Nyquist plots, as depicted in Figure 5. The intersection of the EIS curve with the real axis can be explained by pure ohmic resistance. The semicircle can be attributed to charge transfer

resistance (Rct) and constant phase elements (CPE). The slope line can be ascribed to Warburg impedance (Zw). This is related to lithium ion diffusion between nanoparticles. A smaller semicircle signifies a smaller charge transfer resistance, and a lower slope means a larger lithium-ion-diffusion rate [28]. The resistance value in each equivalent circuit is summarized in Table 1. The Rct value for each electrode was 181.86 Ω (SSZ), 219.6 Ω (PSZ), and 309.39 Ω (SS). The order of the angle in the inclined slope is PSZ>SSZ>SS. Although $SiO_2$ has much greater resistance, it has a higher lithium-ion-diffusion rate than the others. Comprising the SSZ and PSZ electrodes, the resistance (181.86 Ω) of SSZ is much lower than that (219.6 Ω) of PSZ, and the slope of SSZ is lower than that of PSZ. This indicates that the Si-O-Zr bond could be contributing to the conductivity improvement for SSZ, and also that this bond may provide an easier path for charge transfer at the interface between the electrode and electrolyte. Furthermore, from the results in the slope of the lines for SSZ and PSZ, the lithium diffusion rate can be enhanced by the bonds of Si-O-Zr. Therefore, the improved performance of SSZ electrodes would be associated with decrease of the overall internal resistance in a battery and increase in the lithium diffusion rate.

Galvanostatic charge/discharge testing in the voltage range of 0.001 and 2.0V ($Li/Li^+$) at 30mA·$g^{-1}$was employed to investigate the electrical reactivity of each electrode. Figure 6 shows the curve of the charge/discharge profiles for four samples (graphite, SS, PSZ, and SSZ) at different cycles. As the baseline, the capacity of the graphite electrode was measured at the $1^{st}$, $2^{nd}$, and $10^{th}$ cycles (corresponding discharge capacities 448, 337, 318 mAh $g^{-1}$). The discharge capacity of each cycle ($1^{st}$, $2^{nd}$, $5^{th}$, and $10^{th}$) of SS was 952, 290, 269, and 260 mAh $g^{-1}$, respectively, and the corresponding capacities of PSZ were 366, 221, 217, and 200 mAh $g^{-1}$. The SSZ capacities were 1064, 425, 435, and 427 mAh $g^{-1}$ at the $1^{st}$, $2^{nd}$, $5^{th}$, and $10^{th}$ cycles, and it exhibited at capacity of 413 mAh $g^{-1}$ at the $15^{th}$ cycle. The SSZ material with Si-O-Zr bonds exhibited superior capacity compared to SS, PSZ (lacked Si-O-Zr bonding), and graphite. Not only that, but the SSZ also showed better cycling performance than did the graphite. The capacity of SSZ increased from 425 to 438 mAh $g^{-1}$ between the $2^{nd}$ and $8^{th}$ cycles, unlike the capacities of the other electrodes, which declined. There are three possible reasons why the SSZ electrode provided the greatest performance. First, the SSZ could offer facile routes for the electrochemical reactions with lithium ions through the linkage of Si-O-Zr. Second, the Si-O-Zr bond could also shorten the ionic transport length, and third, the ‘Zr’ of the Si-O-Zr bond could possibly suppress SEI formation effectively. The

PSZ electrode showed the lowest capacity of all the electrodes tested, indicating that physically mixed materials without a ternary bond could not transfer each electrochemical reaction due to increasing resistance, and thus it could not duplicate the synergistic effect observed in SSZ.

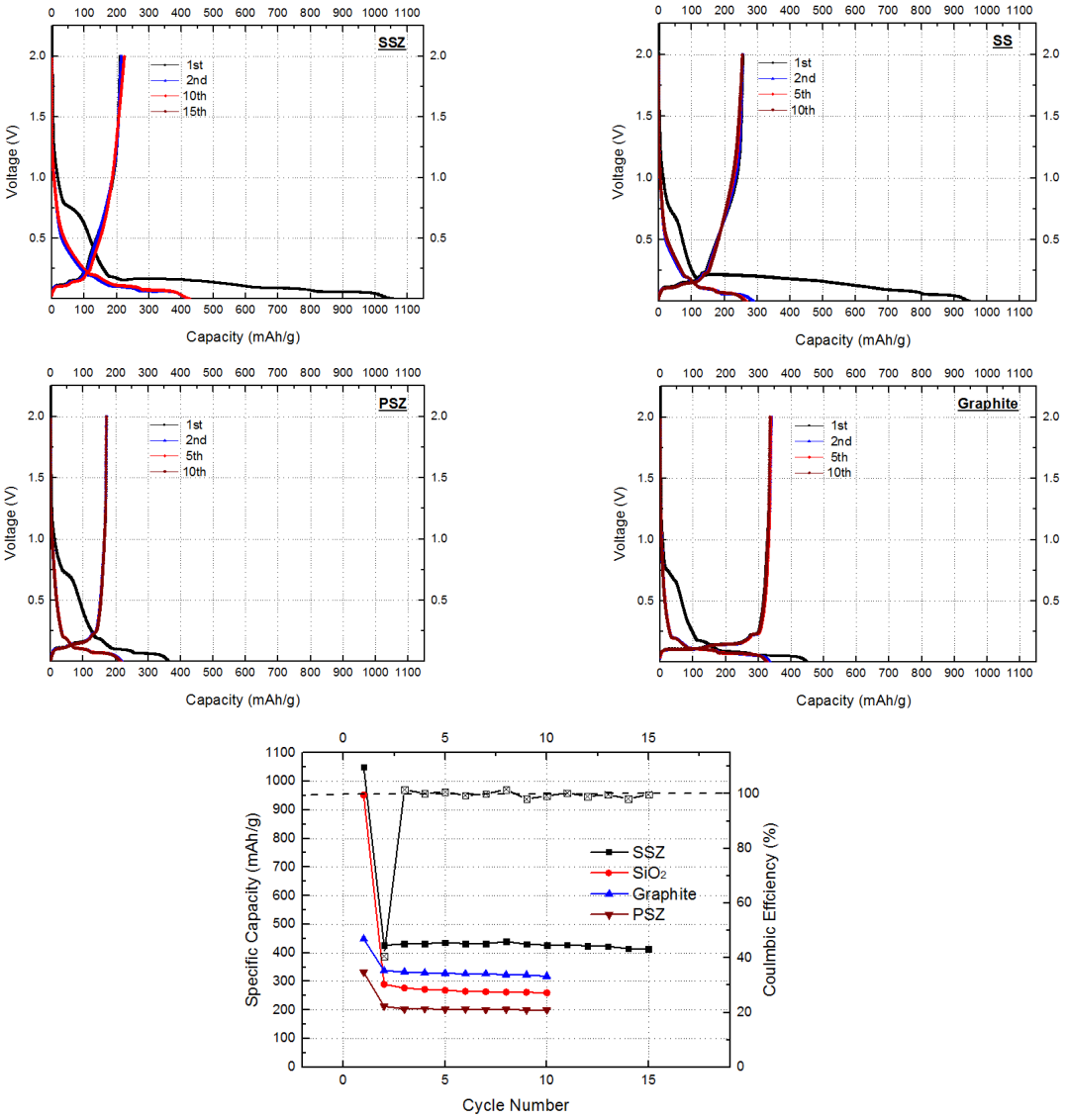


Figure 6. Charge/discharge profiles of: (a) synthesized $SiO_2/ZrO_2$(SSZ); (b) synthesized $SiO_2$; (c) physically mixed $SiO_2$ and $ZrO_2$ (PSZ); (d) graphite; (e) long-term cycling test in the voltage range of 0.001-2.0V

Table 2. Summary of possible electrochemical reactions

| No | Proposed Chemical Reactions |
|---|---|
| 1 | $ZrSiO_4 + 8Li^+ + 8e^- \rightarrow 4Li_2O + ZrSi$<br>$ZrSi + xLi^+ + xe^- \leftrightarrow LixZrSi$ |
| 2 | $ZrSiO_4 + 8Li^+ + 8e^- \rightarrow 4Li_2O + (1/2)Zr_2Si + (1/2)Si$<br>$(1/2)Zr_2Si + xLi^+ + xe^- \leftrightarrow (1/2)LixZr_2Si$ |
| 3 | $ZrSiO_4 + 8Li^+ + 8e^- \rightarrow 4Li_2O + (1/5)Zr_5Si_3 + (2/5)Si$<br>$(1/5)ZrSi + xLi^+ + xe^- \leftrightarrow (1/5)LixZr_5Si_3$ |
| 4 | $2ZrSiO_4 + 8Li^+ + 8e^- \rightarrow 2Li_2ZrO_3 + 2Li_2O + 2Si$ |
| 5 | $2ZrSiO_4 + 4Li^+ + 4e^- \rightarrow 2Li_2SiO_3 + ZrO_2$ |
| 6 | $2ZrSiO_4 + 4Li^+ + 4e^- \rightarrow Li_2Si_2O_5 + Li_2O + ZrO_2$ |

$SiO_2$ is known to have a lower capacity than Si. One of several reasons is that $SiO_2$ structure is based on the strong Si-O bond, which is difficult to break during discharge. The addition of other materials leads to variation of this structural bond and valence charge redistribution. This causes a shift in the core level bonding energy [29]. The $ZrO_2$ synthesis in the $SiO_2$ brings about Si-O-Zr bonding at the interface between the two materials, and this can lead to changes in the strong Si-O bonding during insertion of lithium ions. Furthermore, it can also produce a change in the valence charge. The vulnerability of intrinsic $SiO_2$ (e.g., its low reactivity to lithium ions) can be eclipsed by these changes. When the 1$^{st}$ curves between PSZ and SSZ were compared, there was an obvious difference. The discharge capacities of SSZ and PSZ are 1064 and 366 mAh g$^{-1}$. It is noted that the discharge curves of SSZ were about 2.9 times higher than those of PSZ. This high capacity delivered by the SSZ electrode can be ascribed to the effect of the ternary compounds, which not only increase the packing density, but also create the Si-O-Zr bond that makes additional reactions between $SiO_2$/$ZrO_2$ and Li possible. In the case of PSZ, lithium ions were intercalated into the void between each PSZ ($SiO_2$, $ZrO_2$) particle, but with no connecting linkage. According to the literature, SSZ with Si-O-Zr bonding contains both Lewis and Bronsted acid sites, and the Bronsted acid sites, in particular, offer extra exchange sites [12]. These large exchange sites

help to improve the conductivity of the SSZ. Therefore, the capacity of SSZ is better than that of PSZ. This enhanced conductivity also matches the EIS result in Figure 6. In order that the electrochemical reactions of the SSZ electrode during repeated cycles might be better understood, the possible chemical reactions are summarized in Table 2.

**Conclusions**

A novel anode with high electrochemical performance, made of Earth-abundant $SiO_2/ZrO_2$, and forming Si-O-Zr bonds; was successfully synthesized for use in lithium ion batteries. The electrochemical effects of the Si-O-Zr bonds were investigated. The high capacity and long-term stability of the synthesized SSZ material (Si/Zr=1) with Si-O-Zr bonds was clearly superior when it was compared with the materials (SS, graphite, and the physically mixed material PSZ) that did not have Si-O-Zr bonding. The SSZ electrode with the Si-O-Zr bond delivered a high discharge capacity of 427 mAh $g^{-1}$ after 10 cycles, which means that the capacity of SSZ is 2.1, 1.64, and 1.34 times greater than that of PSZ, SS, or graphite, respectively. This superior capacity and capacity retention are attributed to the effect of the ternary compounds, which contribute not only to increased packing density, but also to creation of the Si-O-Zr bond, which makes additional reactions between $SiO_2/ZrO_2$ and lithium ions possible. The Si-O-Zr bond also contributes to improved conductivity for SSZ and provides facile paths for charge transfer at the electrode/electrolyte interface. The higher electronic conductivity of SSZ with Si-O-Zr bonding was clearly demonstrated using the EIS method. Therefore, the overall internal resistance in a battery would be decreased and better performance could be obtained with SSZ electrodes.

## Reference


1. Dunn, B., H. Kamath, and J.M. Tarascon, *Electrical energy storage for the grid: a battery of choices.* Science, 2011. **334**(6058): p. 928-35.

2. Rao, M., W. Li, and E.J. Cairns, *Porous carbon-sulfur composite cathode for lithium/sulfur cells.* Electrochemistry Communications, 2012. **17**: p. 1-5.

3. Liu, D. and G. Cao, *Engineering nanostructured electrodes and fabrication of film electrodes for efficient lithium ion intercalation.* Energy & Environmental Science, 2010. **3**(9): p. 1218-1237.

4. Fergus, J.W., *Recent developments in cathode materials for lithium ion batteries.* Journal of Power Sources, 2010. **195**(4): p. 939-954.

5. Zhang, Z., et al., *Hierarchical architectured NiS@SiO2 nanoparticles enveloped in graphene sheets as anode material for lithium ion batteries.* Electrochimica Acta, 2015. **155**: p. 85-92.

6. Nan, D., et al., *Highly porous carbon nanofibers from electrospun polyimide/SiO2 hybrids as an improved anode for lithium-ion batteries.* Electrochemistry Communications, 2013. **34**: p. 52-55.

7. Yao, Y., et al., *Carbon-coated SiO2 nanoparticles as anode material for lithium ion batteries.* Journal of Power Sources, 2011. **196**(23): p. 10240-10243.

8. Li, M., et al., *SiO2/Cu/polyacrylonitrile-C composite as anode material in lithium ion batteries.* Journal of Power Sources, 2013. **240**: p. 659-666.

9. Zhang, T., et al., *Preparation and electrochemical properties of core-shell Si/SiO nanocomposite as anode material for lithium ion batteries.* Electrochemistry Communications, 2007. **9**(5): p. 886-890.

10. Liu, J., et al., *Ultrathin atomic layer deposited ZrO2 coating to enhance the electrochemical performance of Li4Ti5O12 as an anode material.* Electrochimica Acta, 2013. **93**(0): p. 195-201.

11. Yi, T.-F., et al., *Spinel Li4Ti5−xZrxO12 (0 ⩽ x ⩽ 0.25) materials as high-performance anode materials for lithium-ion batteries.* Journal of Alloys and Compounds, 2013. **558**: p. 11-17.

12. Tarafdar, A., A.B. Panda, and P. Pramanik, *Synthesis of ZrO2–SiO2 mesocomposite with high ZrO2 content via a novel sol–gel method.* Microporous and Mesoporous Materials, 2005. **84**(1–3): p. 223-228.

13. Parera, J.M., *Promotion of Zirconia Acidity by Addition of Sulfate Ion.* Catalysis Today, 1992. **15**(3-4): p. 481-490.

14. Rao, K.S., et al., *A novel method for synthesis of silica nanoparticles.* Journal of Colloid and Interface Science, 2005. **289**(1): p. 125-131.

15. Wang, S.-W., X.-X. Huang, and J.-K. Guo, *Wet chemical synthesis of ZrO2-SiO2 composite powders.* Journal of the European Ceramic Society, 1996. **16**(10): p. 1057-1061.

16. Castro, Y., et al., *Silica-zirconia sol-gel coatings obtained by different synthesis routes.* Journal of Sol-Gel Science and Technology, 2005. **35**(1): p. 41-50.

17. Monros, G., et al., *Effect of Hydrolysis Time and Type of Catalyst on the Stability of Tetragonal Zirconia Silica Composites Synthesized from Alkoxides.* Journal of Materials Science, 1993. **28**(21): p. 5852-5862.

18. Shalliker, R.A., et al., *A sol-gel preparation of silica coated zirconia microspheres as chromatographic support materials.* Journal of Materials Science, 1997. **32**(11): p. 2949-2955.

19. Parashar, V.K., V. Raman, and O.P. Bahl, *Thermal evolution of sol-gel derived zirconia and binary oxides of zirconia-silica*. Journal of Materials Science Letters, 1996. **15**(18): p. 1625-1629.

20. Bosman, H.J.M., et al., *Characterization of the Acid Strength of Sio2-Zro2 Mixed Oxides.* Journal of Catalysis, 1994. **148**(2): p. 660-672.

21. Nogami, M., *Glass Preparation of the Zro2-Sio2 System by the Sol-Gel Process from Metal Alkoxides.* Journal of Non-Crystalline Solids, 1985. **69**(2-3): p. 415-423.

22. Saha, S.K. and P. Pramanik, *Aqueous Sol-Gel Synthesis of Powders in the Zro2-Sio2 System Using Zirconium Formate and Tetraethoxysilane.* Journal of Non-Crystalline Solids, 1993. **159**(1-2): p. 31-37.

23. Okasaka, K., H. Nasu, and K. Kamiya, *Investigation of Coordination State of Zr4+ Ions in the Sol Gel-Derived Zro2-Sio2 Glasses by Exafs.* Journal of Non-Crystalline Solids, 1991. **136**(1-2): p. 103-110.

24. Lopez, T., et al., *Preparation of Sol-Gel Sulfated Zro2-Sio2 and Characterization of Its Surface-Acidity.* Applied Catalysis a-General, 1995. **125**(2): p. 217-232.

25. Schroder, K.W., et al., *Examining Solid Electrolyte Interphase Formation on Crystalline Silicon Electrodes: Influence of Electrochemical Preparation and Ambient Exposure Conditions.* The Journal of Physical Chemistry C, 2012. **116**(37): p. 19737-19747.

26. Zhang, X.N., et al., *Si–AB5 composites as anode materials for lithium ion batteries.* Electrochemistry Communications, 2007. **9**(4): p. 713-717.

27. Ren, Y., et al., *Preparation and characterization of silicon monoxide/graphite/carbon nanotubes composite as anode for lithium-ion batteries.* Journal of Solid State Electrochemistry, 2012. **16**(4): p. 1453-1460.

28. Armstrong, R.D. and H. Wang, *Behaviour of nickel hydroxide electrodes after prolonged potential float.* Electrochimica Acta, 1991. **36**(5–6): p. 759-762.

29. Chang, W.-S., et al., *Quartz (SiO2): a new energy storage anode material for Li-ion batteries.* Energy & Environmental Science, 2012. **5**(5): p. 6895-6899.